ELECTRONIC SUPPORTING INFORMATION (ESI)

Structural adaptations of electrosprayed aromatic oligoamide foldamers on Ag(111)

Dennis Meier,[a] Benedikt Schoof,[a] Jinhua Wang,[b] Xuesong Li,[b] Andreas Walz,[a] Annette Huettig,[a] Hartmut Schlichting,[a] Frédéric Rosu,[c] Valérie Gabelica,[d] Victor Maurizot,[b] Joachim Reichert,[a] Anthoula C. Papageorgiou,*[a] Ivan Huc*[e,f] and Johannes V. Barth[a,f]

[a]*Physics Department E20, Technical University Munich, D-85748 Garching, Germany. E-mail: a.c.papageorgiou@tum.de*
[b]*CBMN (UMR 5248), Univ. Bordeaux, CNRS, Bordeaux INP, F-33600 Pessac, France.*
[c]*Institut Européen de Chimie et Biologie (UAR3033/US001), Univ. Bordeaux, CNRS, INSERM, F-33600 Pessac, France.*
[d]*ARNA (U1212), Univ. Bordeaux, INSERM, CNRS, F-33600 Pessac, France.*
[e]*Department of Pharmacy, Ludwig-Maximilians-University Munich, D-81377 Munich, Germany. Email: ivan.huc@cup.lmu.de*
[f]*Cluster of Excellence e-conversion, D-85748 Garching, Germany.*

Table of Contents

1. Synthetic procedures

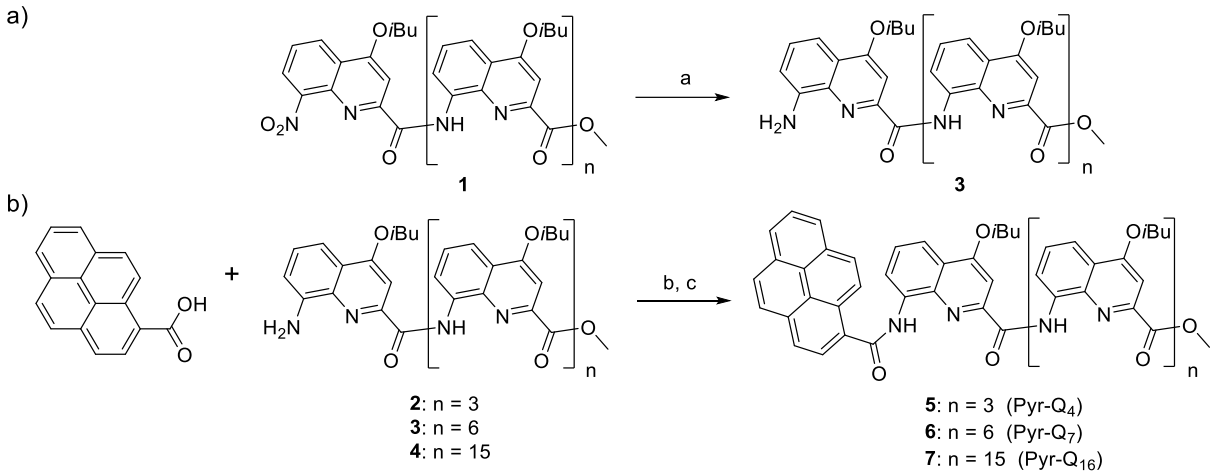

Scheme S1. synthesis of oligomer **5**, **6** and **7** with pyrene group at N-terminus. a: NH_4HCO_2, NH_4VO_3, Pd/C (10%), ethyl acetate, ethanol, water, reflux; b: $CHCl_3$ 1-chloro-N,N,2-trimethyl-1-propenylamine; c: $CHCl_3$, DIEA, r.t.

Free amine oligomers **2** and **4** have been reported previously.[1] Oligomer **1** with $–NO_2$ group at N-terminus has been reported before.[2]

General Remarks: All the solvents and reagents were used as received from commercial suppliers without further purifications unless otherwise specified. Dry chloroform and dry diisopropylethylamine (DIEA) were distilled from calcium hydride before use. ^{1}H NMR, ^{13}C NMR spectra were recorded on BRUKER AVANCE 300 MHz spectrometers. Chemical shifts were presented in parts per million (δ, ppm) using solvent residue peaks as references (chloroform δ = 7.26 ppm). Coupling constants are reported as Hertz. Reactions were monitored by thin layer chromatography (TLC) on Merck silica gel 60-F254 plates and observed under UV light. Silica gel column chromatography purifications were carried out on Merck GEDURAN Si60 (40-63 μm). Preparative recycling Gel Permeation Chromatography (GPC) was performed on a JAI LC-9130G NEXT using two JAIGEL 20×600 mm columns (Japan Analytical Industry) with 0.5 % NEt_3 and 1% ethanol in chloroform (HPLC grade, ethanol stabilized), as mobile phase, with a flow rate of 7 mL/min. ESI mass spectra were obtained from the Mass Spectrometry Laboratory at the European Institute of Chemistry and Biology (UMS 3033 - IECB), Pessac, France.

Compound 2: oligomer **1** (1.5 g, 0.85 mmol), NH_4HCO_2 (2.69 g, 42.7 mmol), NH_4VO_3 (43 mg, 0.38 mmol) was added into a dry flask. A mixture of solvents: ethyl acetate/ethanol/water (80 mL/19 mL/3.8 mL) was added into the flask to dissolve the oligomer. The Pd/C (10%, 120 mg) was added into the mixture while stirring at room temperature. The mixture was then heated at 75 °C under N_2 for overnight. After cooling down to room temperature, 40 mL of dichloromethane was added to dilute the solution and filtrate through a pack of celite® to remove the Pd/C catalyst. The solution was then washed with 5% ammonium chloride solution two times (40 mL per time). The organic layer was separated and dried over sodium sulfate.

After filtration and removing the solvent, a yellow solid was obtained. The yield of the reaction was quantitative as indicated by the crude ^{1}H NMR spectra and the product was used for subsequent reaction without any further purifications. ^{1}H NMR (300 MHz, $CDCl_3$): δ 11.71 (s, 1H), 11.54 (s, 1H), 11.51 (s, 1H), 11.28 (s, 1H), 11.22 (s, 1H), 11.13 (s, 1H), 8.28 (d, *J* = 8.0 Hz, 1H), 8.18 (d, *J* = 7.9 Hz, 1H), 8.14 (d, *J* = 8.0 Hz, 1H), 8.12 (d, *J* = 8.0 Hz, 1H), 8.05 (dd, *J* = 8.4, 1.3 Hz, 1H), 7.96 (d, *J* = 8.2 Hz, 1H), 7.95 (d, *J* = 8.2 Hz, 1H), 7.91 (dd, *J* = 8.4, 1.3 Hz, 1H), 7.84 (dd, *J* = 8.4, 1.3 Hz, 1H), 7.81 (dd, *J* = 8.3, 1.3 Hz, 1H), 7.71 (dd, *J* = 7.8, 1.2 Hz, 1H), 7.60 (dd, *J* = 7.8, 1.3 Hz, 1H), 7.47 (d, *J* = 3.1 Hz, 1H), 7.44 (d, *J* = 3.0 Hz, 1H), 7.43 – 7.24 (m, 4H), 7.22 – 7.18 (m, 2H), 6.99 (s, 1H), 6.94 (s, 1H), 6.90 (t, *J* = 7.6 Hz, 1H), 6.81 (s, 1H), 6.66 (s, 1H), 6.56 (s, 1H), 6.55 (s, 1H), 6.48 (s, 1H), 5.78 (d, *J* = 7.6 Hz, 1H), 4.21 – 3.80 (m, 12H), 3.76 (d, *J* = 6.3 Hz, 2H), 3.09 (s, 3H), 2.59 – 2.14 (m, 7H), 1.39 – 1.08 (m, 42H) ppm.

General Procedure for the acid chloride coupling reaction: 1-pyrenecarboxylic acid (1.1 equiv. with respect to the amine oligomers) was dissolved in dry $CHCl_3$ (3 mL/100 mg). Activation reagent (1.3 equiv.), 1-chloro-N,N,2-trimethyl-1-propenylamine, was added into the solution. The mixture was stirred at room temperature under N_2 for about 2 hours. Solvent and residue excess activation reagent were removed under high vacuum. The solid of 1-pyrenecarboxylic acid chloride was dried under high vacuum for additional 3 hours. The amine oligomer was added into a separated dry flask and sealed under N_2. The dry 1-pyrenecarboxylic acid chloride was dissolved in a minimum amount of dry $CHCl_3$ (around 3 mL) and transferred into the flask containing the amine oligomers. Dry DIEA was added into the mixture. The reaction mixture was stirred at room temperature under N_2 for overnight. After complete of reaction, the solvent was removed, and the residue was purified with GPC or silica gel chromatography when necessary and followed by precipitation with dichloromethane/MeOH mixture.

Oligomer 5 (pyr-Q$_4$): The compound was synthesized following the general procedure, starting with amine **2** (100 mg, 0.1 mmol) and 1-pyrenecarboxylic acid (27 mg, 0.11 mmol). Yield: 105 mg (85%). ^{1}H NMR (300 MHz, $CDCl_3$): δ: 11.67 (s, 1H), 11.41 (s, 1H), 11.38 (s, 1H), 9.93 (s, 1H), 8.52 (dd, *J* = 7.6, 1.3 Hz, 1H), 8.37 (dd, *J* = 7.6, 1.3 Hz, 1H), 8.28 (dd, *J* = 7.9, 2.6 Hz, 2H), 8.22 (d, *J* = 7.0 Hz, 1H), 8.19 (d, *J* = 7.6 Hz, 1H), 8.07 – 8.02 (m, 4H), 8.01 (dd, *J* = 8.2, 1.2 Hz, 1H), 7.96 (dd, *J* = 8.6, 1.3 Hz, 1H), 7.94 (d, *J* = 7.8 Hz, 1H), 7.73 (t, *J* = 8.0 Hz, 1H), 7.66 (t, *J* = 8.0 Hz, 1H), 7.53 – 7.45 (m, 3H), 7.40 (t, *J* = 8.0 Hz, 1H), 7.25 (t, *J* = 6.6 Hz, 1H), 7.20 (t, *J* = 8.0 Hz, 1H), 6.86 (d, *J* = 7.5 Hz, 1H), 6.78 (s, 1H), 6.41 (s, 1H), 6.26 (s, 1H), 4.43 (dd, *J* = 9.0, 6.2 Hz, 1H), 4.29 – 4.18 (m, 1H), 3.96 – 3.82 (m, 2H), 3.74 (m, 4H), 3.04 (s, 3H), 2.60 – 2.22 (m, 4H), 1.41 – 1.11 (m, 24H) ppm; ^{13}C NMR (75 MHz, CDCl3): δ 166.08, 163.96, 163.73, 163.37, 162.26, 161.91, 161.04, 160.95, 160.66, 150.37, 149.12, 148.33, 145.28, 139.01, 138.36, 138.15, 137.03, 134.10, 133.80, 133.53, 133.27, 132.78, 130.51, 129.75, 129.25, 128.86, 128.39, 128.23, 127.97, 127.70, 127.55, 127.31, 126.95, 126.37, 125.69, 125.48, 125.25, 124.98, 124.24, 123.84, 123.20, 122.55, 121.80, 121.74, 120.92, 117.98, 117.43, 117.06, 116.74, 116.51, 116.45, 115.99, 115.58, 100.17, 99.52, 97.71, 96.41, 75.74, 75.31, 74.99, 52.13, 28.43, 28.36, 28.30, 19.86, 19.64, 19.62, 19.54, 19.51, 19.48, 19.43 ppm; ESI+ HRMS m/z: calcd for $C_{74}H_{69}N_8O_{10}$ $[M+H]^+$ 1229.5137, found 1229.5147.

Oligomer 6 (pyr-Q_7): The compound was synthesized following the general procedure, starting with amine **3** (18 mg, 0.01 mmol) and 1-pyrenecarboxylic acid (3 mg, 0.011 mmol). Yield: 15 mg (76%). ^{1}H NMR (300 MHz, $CDCl_3$): δ 11.44 (s, 1H), 11.31 (s, 1H), 10.84 (s, 2H), 10.80 (s, 1H), 10.37 (s, 1H), 9.51 (s, 1H), 8.22 (d, *J* = 7.0 Hz, 1H), 8.10 (d, *J* = 8.2, 1.3 Hz, 1H), 8.07 (d, *J* = 8.2, 1.3 Hz, 1H), 8.03 – 7.92 (m, 3H), 7.92 – 7.86 (m, 4H), 7.86 – 7.73 (m, 4H), 7.71 – 7.59 (m, 4H), 7.47 – 7.28 (m, 7H), 7.14 (t, *J* = 7.9 Hz, 1H), 7.06 (d, *J* = 8.8 Hz, 1H), 7.04 (s, 1H),6.95 (d, *J* = 9.4 Hz, 1H), 6.88 (t, *J* = 8.0 Hz, 1H), 6.70 (d, *J* = 7.5 Hz, 1H), 6.64 (s, 1H), 6.61 (s, 1H), 6.50 (s, 1H), 6.33 (s, 2H), 5.64 (s, 1H), 4.22 – 3.39 (m, 14H), 2.97 (s, 3H), 2.59 – 2.03 (m, 7H), 1.48 – 1.02 (m, 42H) ppm; ^{13}C NMR (75 MHz, CDCl3): δ 165.97, 163.73, 163.45, 162.96, 162.81, 161.97, 161.28, 161.24, 160.65, 160.46, 159.53, 159.01, 158.47, 149.79, 149.25, 148.90, 148.81, 147.47, 145.09, 138.71, 138.11, 137.89, 137.75, 137.53, 137.41, 136.75, 133.64, 133.42, 133.13, 132.93, 132.80, 132.73, 132.46, 130.18, 129.50, 129.01, 128.37, 127.96, 127.74, 127.54, 127.31, 126.90, 126.74, 126.46, 125.85, 125.71, 125.55, 125.14, 125.00, 124.82, 123.77, 123.40, 122.85, 122.50, 122.28, 121.72, 121.46, 121.38, 121.25, 117.71, 116.84, 116.55, 116.38, 116.23, 116.07, 115.55, 115.36, 100.12, 99.36, 98.88, 98.53, 97.77, 97.47, 77.59, 77.17, 76.74, 75.50, 75.42, 75.13, 74.79, 53.58, 52.03, 45.97, 28.40, 28.27, 28.21, 20.02, 19.80, 19.68, 19.65, 19.63, 19.59, 19.53, 19.44, 19.38, 19.36, 19.25, 8.76 ppm; ESI+ HRMS m/z: calcd for $C_{116}H_{111}N_{14}O_{16}$ $[M+H]^+$ 1956.8336, found 1956.8320.

Oligomer 7: The compound was synthesized following the general procedure, starting with amine **4** (20 mg, 0.005 mmol) and 1-pyrenecarboxylic acid (1.5 mg, 0.006 mmol). Yield: 16 mg (68%). ^{1}H NMR (300 MHz, $CDCl_3$): δ 11.10 (s, 1H), 11.05 (s, 1H), 10.47 (s, 1H), 10.31 (s, 1H), 10.26 (s, 1H), 10.11 (s, 1H), 10.06 (s, 1H), 10.02 (s, 1H), 9.95 (s, 1H), 9.92 (s, 1H), 9.90 (s, 1H), 9.88 (s, 1H), 9.85 (s, 2H), 9.77 (s, 1H), 9.05 (s, 1H), 7.93 (d, *J* = 7.5 Hz, 1H), 7.87 (d, *J* = 7.4 Hz, 1H), 7.81 (d, *J* = 8.9 Hz, 1H), 7.78 – 7.70 (m, 4H), 7.69 – 7.61 (m, 7H), 7.60 – 7.49 (m, 6H), 7.46 (d, *J* = 7.9 Hz, 1H), 7.21 (d, *J* = 7.5 Hz, 3H), 7.16 (d, *J* = 8.1 Hz, 2H), 7.13 – 6.63 (m, 28H), 6.51 (d, *J* = 7.5 Hz, 1H), 6.40 (s, 1H), 6.37 (s, 1H), 6.20 (s, 1H), 6.15 (s, 1H), 6.12 (s, 1H), 5.86 (s, 1H), 5.74 (s, 1H), 5.73 (s, 1H), 5.71 (s, 2H), 5.68 (s, 2H), 5.65 (s, 2H), 5.37 (s, 1H), 4.01 – 3.40 (m, 30H), 3.28 (t, *J* = 8.2 Hz, 2H), 2.82 (s, 3H), 2.39 – 1.98 (m, 16H), 1.23 – 0.97 (m, 64H), 0.87 (q, *J* = 7.9, 7.2 Hz, 8H) ppm; ^{13}C NMR (75 MHz, $CDCl_3$) δ 165.72, 165.25, 163.64, 163.09, 162.64, 162.45, 162.30, 162.22, 162.12, 161.79, 161.68, 161.61, 160.86, 160.39, 160.04, 158.91, 158.70, 158.64, 158.55, 158.51, 158.43, 158.32, 158.16, 157.89, 149.47, 148.70, 148.45, 148.42, 148.03, 147.88, 147.87, 147.20, 144.87, 138.55, 137.79, 137.51, 137.06, 136.83, 136.78, 136.67, 136.56, 136.27, 133.45, 133.05, 132.89, 132.73, 132.37, 132.34, 132.12, 131.94, 129.18, 127.64, 126.62, 125.50, 125.35, 122.11, 121.75, 121.54, 121.45, 121.41, 121.32, 121.11, 120.85, 116.58, 116.35, 115.96, 115.60, 115.37, 115.14, 98.14, 75.05, 74.83, 53.57, 51.90, 45.90, 28.14, 28.06, 27.98, 19.94, 19.72, 19.69, 19.60, 19.58, 19.51, 19.44, 19.36, 19.30, 19.20, 19.21, 8.75 ppm; ESI+ HRMS m/z: calcd for $C_{242}H_{238}N_{32}O_{34}$ $[M+2H]^{2+}$ 2068.8972, found 2068.8951.

2. Crystallography

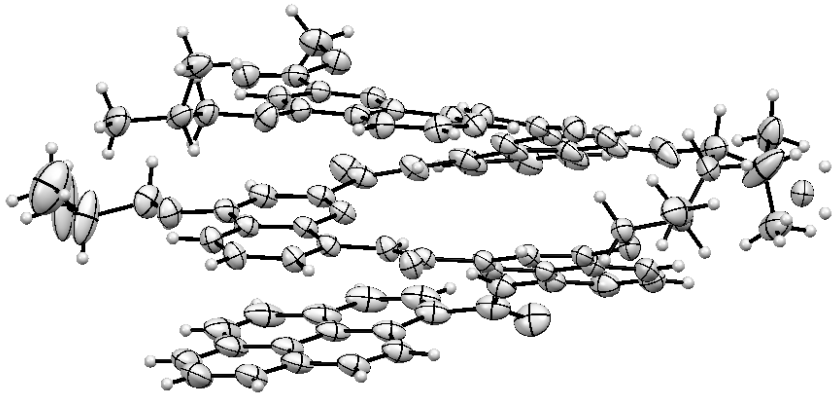

Figure S1. Ortep representation of the structure of compound **5**.

Single crystals of compound **5** were grown by slow diffusion of methanol into a stock solution in $CHCl_3$. A suitable crystal was selected and mounted on a Rigaku FRX diffractometer. The crystal was kept at 130 K during data collection. Using Olex2[3], the structure was solved with the SHELXT[4] structure solution program using Intrinsic Phasing and refined with the SHELXL[5] refinement package using Least Squares minimization.

Table S1: Crystal data and structure refinement

Identification code	wj_pyQ4_ref_b
Empirical formula	$C_{74}H_{68}N_8O_{10}$
Formula weight	1229.36
Temperature/K	130
Crystal system	triclinic
Space group	P-1
a/Å	12.1814(2)
b/Å	16.7246(3)
c/Å	17.9169(3)
α/°	110.870(2)
β/°	91.168(2)
γ/°	99.895(2)
Volume/Å^3	3346.74(11)
Z	2
ρ_{calc}g/cm^3	1.220
μ/mm^{-1}	0.665
F(000)	1296.0
Crystal size/mm^3	0.1 × 0.1 × 0.1
Radiation	CuKα (λ = 1.54178)

2Θ range for data collection/°	5.762 to 140.134
Index ranges	$-14 \leq h \leq 14$, $-20 \leq k \leq 19$, $-19 \leq l \leq 21$
Reflections collected	39409
Independent reflections	12525 [R_{int} = 0.0151, R_{sigma} = 0.0125]
Data/restraints/parameters	12525/6/850
Goodness-of-fit on F^2	1.041
Final R indexes [I>=2σ (I)]	R_1 = 0.0560, wR_2 = 0.1585
Final R indexes [all data]	R_1 = 0.0577, wR_2 = 0.1601
Largest diff. peak/hole / e $Å^{-3}$	1.10/-0.49
CCDC number	2143687

3. Scanning tunneling microscopy (STM)

An Aarhus-type variable temperature STM (Specs GmbH) in a homemade UHV system (base pressure 2×10^{-10} mbar) connected to the ES-CIBD system was used for the study in the Technical University of Munich. The reported STM images were acquired with an electrochemically etched W tip. The tunnelling parameters and the sample temperature are reported along with the STM data, where the bias refers to the sample bias.

4. Surface preparation

4.1 Electrospray ionisation

The foldamers were solved in a mixture of acetonitrile (69 vol%) methanol (29 vol%) and acetic acid (2 vol%). The methanol was added for stabilizing the spray of the foldamer solution. The sprayed solutions had a concentration between 10^{-4} to 10^{-5} mol/l. The ESI emitter was a fused silica capillary with inner and outer diameter of 0.075 mm and 0.360 mm, respectively. The emitter voltage was set to ~ 5 kV and the flow rate to 60–90 µl/h. The pressure during the depositions was lower than 5×10^{-10} mbar. Due to a low signal-to-noise ratio in the mass spectrum of spectrum of pyr-Q_7, a 10-point average fit was applied to the spectrum presented in manuscript Figure 1g (see Figure S2 below for raw data).

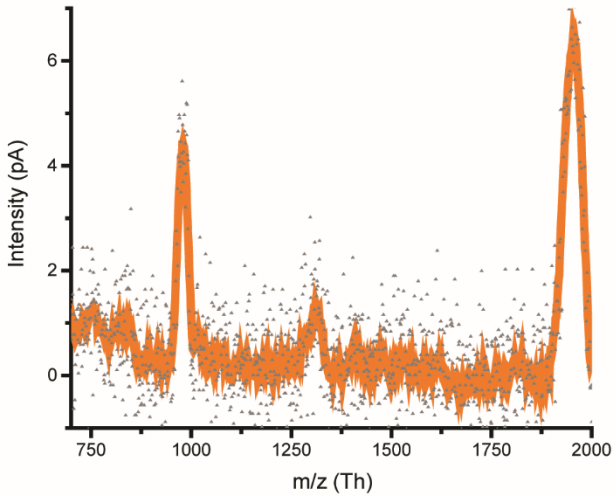

Figure S2. Mass spectrum of pyr-Q_7 prior to the deposition. Original data in grey and 10-points average fit in orange.

The Rayleigh limit provides an upper limit of the charge carried by a droplet.[6] Higher charging leads to a Coulomb repulsion greater than surface tension and triggers Coulomb fission. As electrospray ions originate from such charged droplets, the Rayleigh limit also provides valuable information on the conformation of ions due to their charge states: the charge depends on the apparent surface which is determined by the molecule's geometry. The surface tension of a solution of acetonitrile (69 vol%) and methanol (29 vol%) can be estimated as $\gamma \sim 25\ \mathrm{mN}/m$.[7] Further, assuming a density of $\rho \sim 1.22\ \mathrm{g/cm^3}$ as in the single crystal (see Table S1), we can approximate the sizes of the foldamers. In the helical form, pyr-Q_4 and pyr-Q_7 have aspect ratios close to unity and may therefore be approximated by spherical droplets of

approximately 0.74 nm and 0.86 nm radius. The resulting maximum charges of 1.5 e and 1.9 e coincide with the measured charge states of pyr-Q_4 (exclusively singly charged, manuscript Figure 1f) and pyr-Q_7 (preferably singly charged with additional doubly charged species of lower abundance, manuscript Figure 1g), respectively. For a completely unfolded and stretched molecule having an elongated cylindrical (elliptical) shape, one would expect slightly higher charging due to the larger surface and length and therefore lower Coulomb repulsion between the charge carriers. These calculations, in combination with the ion mobility measurements of section 5, suggest a cylindrical molecule compatible with a helix structure in the gas phase (vacuum).

4.2 Deposition

The Ag(111) crystal substrate was prepared prior to deposition, *in situ* by multiple cycles of Ar^+ sputtering (1 kV, 30 μA sample current, 10 min) and annealing (650 K, 20 min). The cleanliness of the substrate was assessed by STM. A deposition of a $[\text{pyr-}Q_4\text{+H}]^+$ total charge of 43 nC (~ $2.7\cdot10^{11}$ molecules) revealed solely the decoration of the step edges and their vicinity (see Figure S3a below). For pyr-Q_4, 2D islands on Ag(111) were firstly observed by STM after a deposition of a total charge of 114 nC (~ $7.2\cdot10^{11}$ molecules) and these were extended to more than 60 nm long (see Figure S3b) after a deposition of a total charge of 325 nC (~ $2.0\cdot10^{12}$ molecules). For pyr-Q_7, the decoration of the step edges with adsorbed islands was observed by STM after a deposition of a total charge of 155 nC (~ $9.7\cdot10^{11}$ molecules). No pyr-Q_7 molecules were imaged at the terraces at temperatures of 120 K or higher.

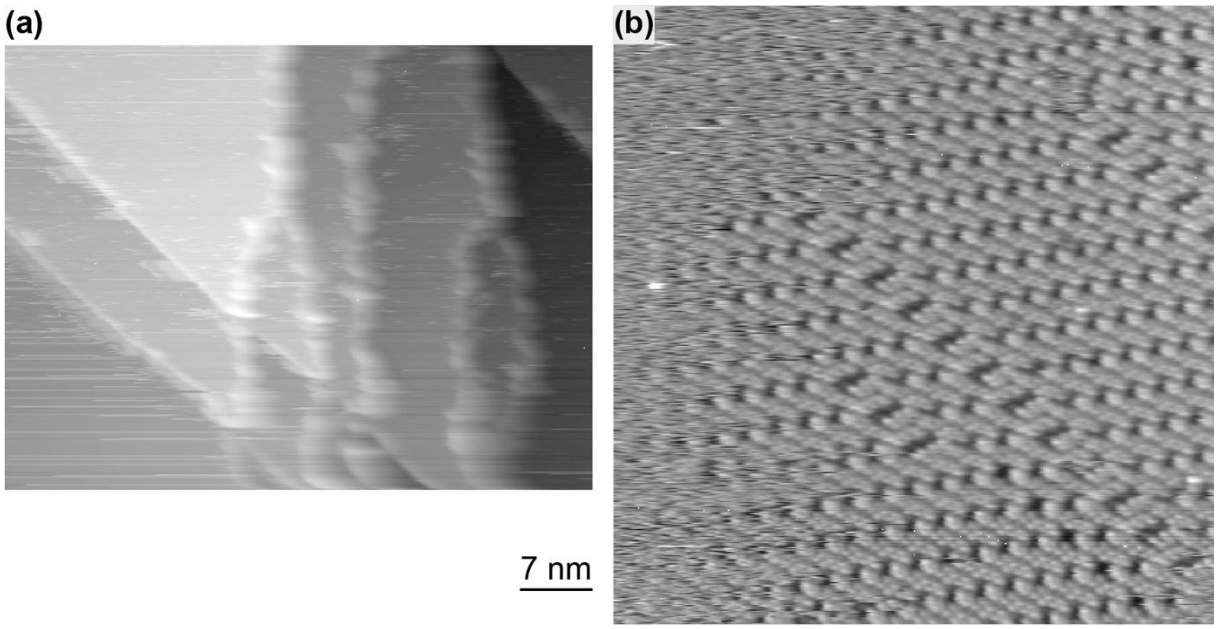

Figure S3. (a) STM image of a $[\text{pyr-}Q_4\text{+H}]^+$ deposition with total charge 43 nC (2500 mV, 50 pA, 180 K). Molecules are only observed on the step edges. (b) STM image (1500 mV, 50 pA, 170 K) of a $[\text{pyr-}Q_4\text{+H}]^+$ deposition with a total charge of 325 nC. A self-assembled island extending to more than 60 nm is depicted. The island borders with diffusing adsorbates on the planar surface.

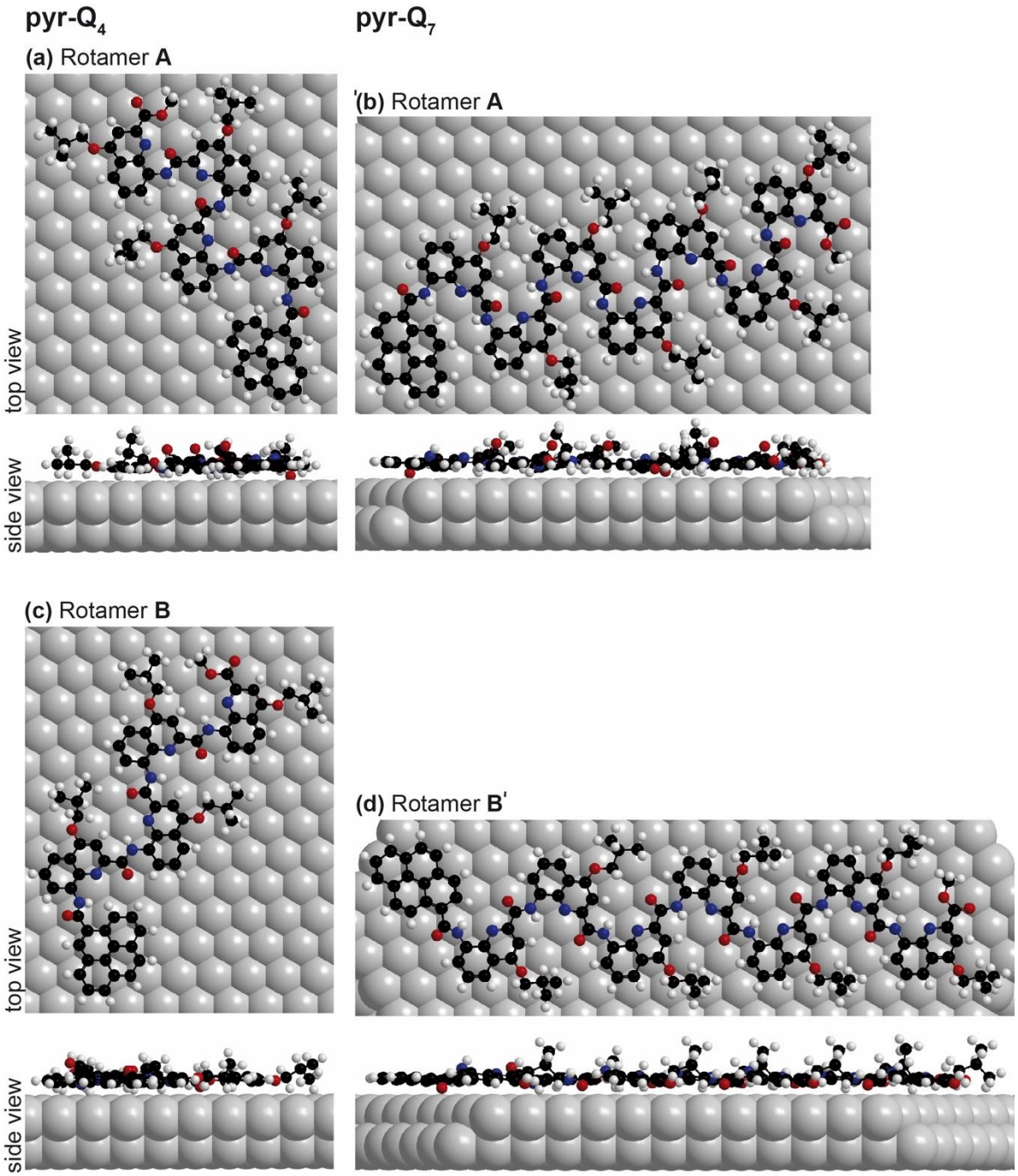

Figure S4. Geometry optimisations (MM+) of pyr-Q_4 and pyr-Q_7 on Ag(111) in ball-and-stick representation. (a) Rotamer **A** of pyr-Q_4 was obtained by rotation of the aryl-NH bonds between the quinoline monomers. (b) Rotamer **B** of pyr-Q_4 obtained by rotation of the aryl-carbonyl bonds between the quinoline monomers. (c) Rotamer **A′** of pyr-Q_7 obtained by rotation of the aryl-NH bonds between the quinoline monomers. (d) Rotamer **B′** of pyr-Q_7 obtained by rotation of the aryl-carbonyl bonds between the quinoline monomers. C, N, O, H and Ag atoms in black, blue, red, white and silver, respectively.

5. Ion mobility (native) mass spectrometry

Experiments were performed on an Agilent 6560 DTIMS-Q-TOF instrument (Agilent Technologies, Santa Clara, CA), with the dual-ESI source operated in the positive ion mode. A CH_2Cl_2/MeOH (4:1 vol/vol) solution was used. A syringe pump flow rate of 190 µL/h and a standard electrospray with a stainless-steel needle with a 0.25 mm internal bore was used. Capacitance diaphragm gauges are connected to the funnel vacuum chamber and to the drift tube. An in-house modification to the pumping system allows better equilibration of the pressures: an Edwards E2M40 vacuum pump (Edwards, UK) is connected to the source region with two Edwards SP16K diaphragm valves connected to the front pumping lines, while an Edwards E2M80 vacuum pump is connected to the Q-TOF region. The helium pressure in the drift tube was 3.89 ± 0.01 Torr, and the pressure in the trapping funnel was 3.79 ± 0.01 Torr. The pressure differential between the drift tube and the trapping funnel ensures only helium is present in the drift tube. The acquisition software version was B.09.00. All spectra were recorded using soft source conditions. The tuning parameters of the instrument (electrospray source, trapping region and post-IMS region (QTOF region)) are optimized as described elsewhere.[8] The source temperature was set at 220 °C and the source fragmentor voltage was set to 350 V. The trapping time was 1000 µs and release time 200 µs. Trap entrance grid delta was set to 2 V

Step-field experiments (five drift tube voltages for each sample) were performed to determine the collision cross sections (CCS, Figure S5). The arrival time t_A is related to DV (voltage difference between the entrance and the exit of the drift tube region) by:

$$t_A = \frac{L^2}{K_0}\frac{T_0 p}{p_0 T}\cdot\left(\frac{1}{\Delta V}\right) + t_0$$

t_0 is the time spent outside the drift tube region and before detection. A graph of t_A vs. 1/DV provides K_0 from the slope and t_0 as the intercept. The drift tube length is L = 78.1 ± 0.2 cm, the temperature is measured accurately by a thermocouple (T = 297 ± 1 K), and the pressure is measured by a capacitance gauge (p = 3.89 ± 0.01 Torr). The CCS is determined using:

$$CCS = \frac{3ze}{16N_0}\cdot\sqrt{\frac{2\pi}{\mu k_B T}}\cdot\frac{1}{K_0}$$

The relative combined standard uncertainty on the CCS of the peak center is ~2.0%.[9] The reconstruction of the experimental CCS distributions from the arrival time distributions at the lowest voltage is then performed using equation:

$$CCS = a\cdot\frac{z}{\sqrt{\mu}}\times t_A$$

where the factor *a* is determined from the t_A of the peak center at the lowest voltage and the CCS calculated from the regression described above, from the peak centers.

6. Calculation of gas-phase structures and collision cross sections (CCS) by molecular dynamics

Molecular dynamics simulations were used to calculate theoretical collision cross sections of the gas-phase foldamers. The crystal structure of Q_8 was used as a starting model. To reach the experimental charge state (1+), a proton was added to the N of the quinoline (at the C-terminus). To reach higher charge states (2+ to 4+), protons were added on the carbonyl group of the linker between the quinoline. The charges used for the calculation of the structures and CCS values were: Q4: 1+, Q8: 1+, Q16: 2+, and Q32: 3+. The proposed protonation sites have been determined by DFT calculation (data not shown). The structures were optimised at the DFT level for Q_4 and Q_8 and because of the size of Q_{16} and Q_{32} at the semi-empirical level PM7[10] using Gaussian 16 rev. B.01.[11] Then, Atom-Centered Density Matrix Propagation molecular dynamics (ADMP, 2000 fs, 296 K) at the DFT or semi-empirical level (PM7) were performed. The theoretical CCS values were calculated for a structure every 10 fs, using the trajectory model (Mobcal[12], original parameters for helium). A histogram of the calculated CCS is made using Sigmaplot 14 (Figure S5).

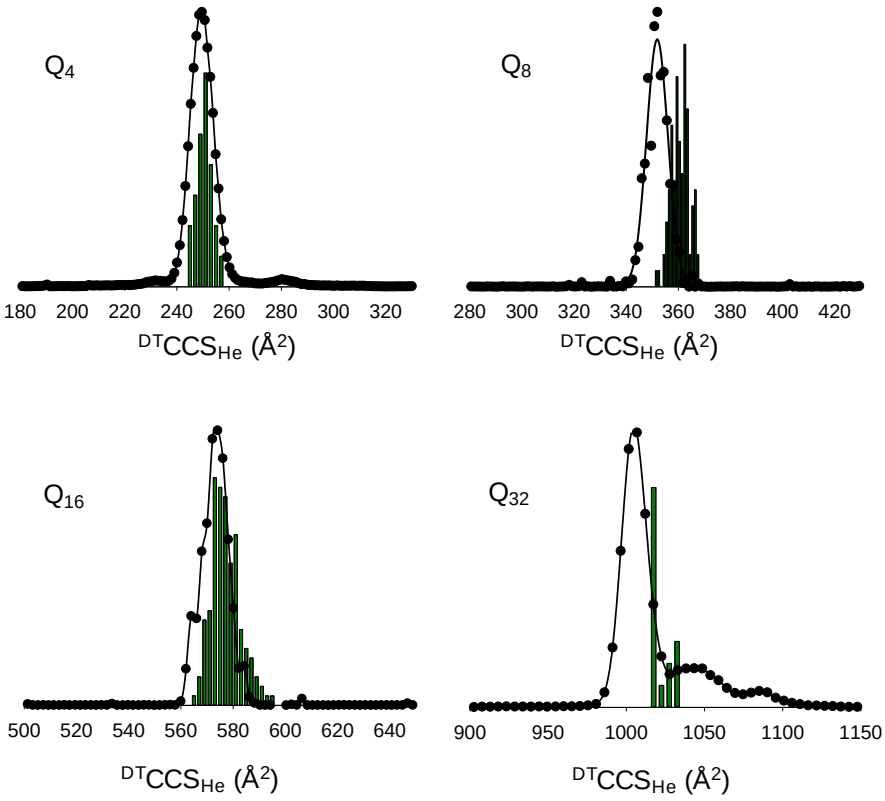

Figure S5. Collision cross sections ($^{DT}CCS_{He}$) of the different foldamers species measured by drift tube ion mobility ESI-MS. The corresponding theoretical CCSs calculated from snapshots sampled from ab-initio molecular dynamics simulations is displayed as histograms. For Q_4 and Q_8, DFT level (MO62X, 6-31G*) is used. Because of the size of Q_{16} and Q_{32}, semi-empirical level (PM7) is used.

7. NMR and MS spectra

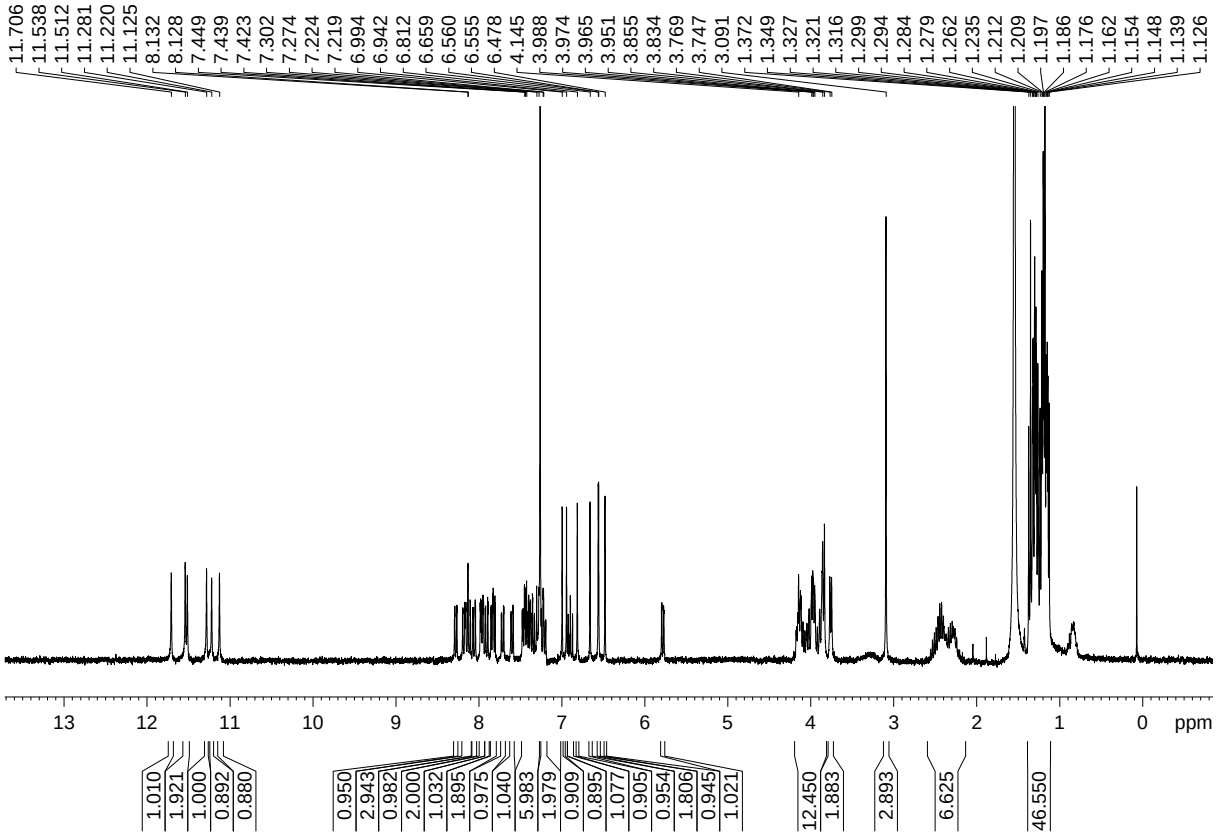

Figure S6. ^{1}H NMR spectrum (300 MHz, $CDCl_3$) of oligomer **3**.

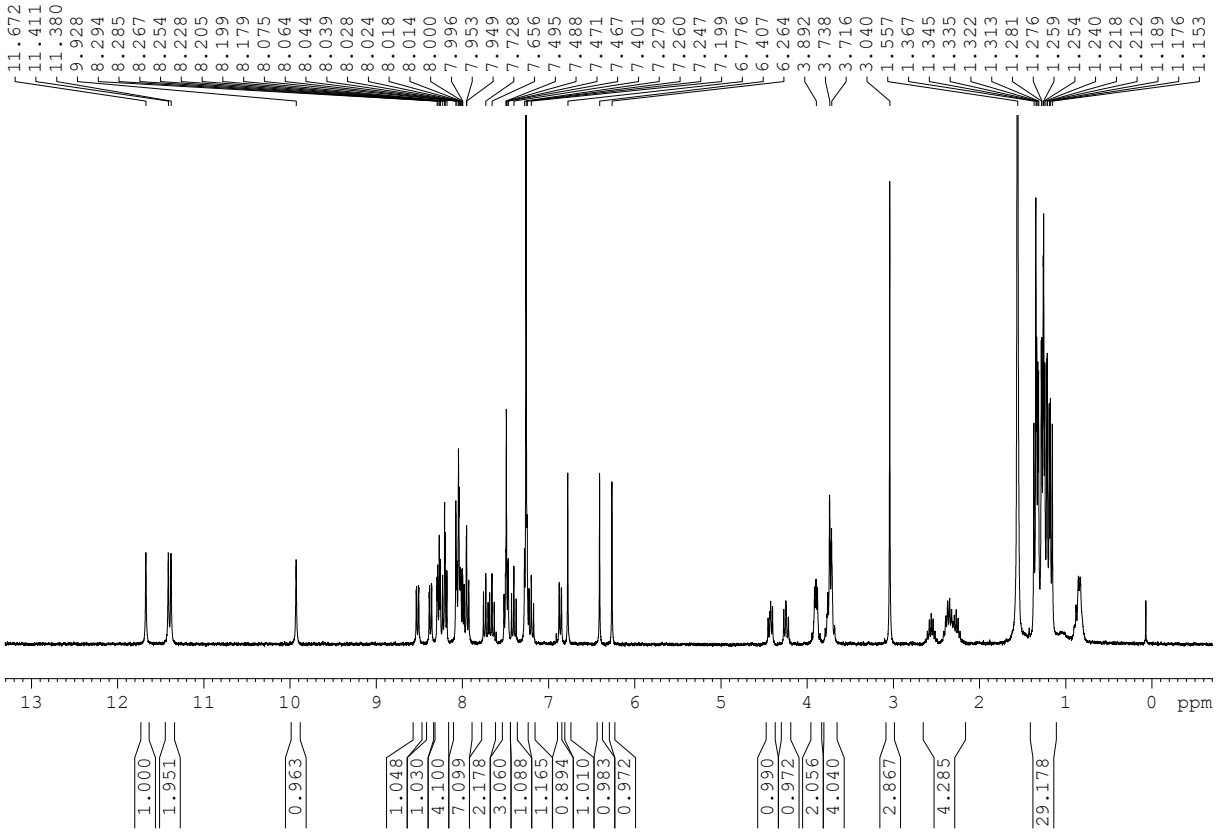

Figure S7. ^{1}H NMR spectrum (300 MHz, $CDCl_3$) of oligomer **5**.

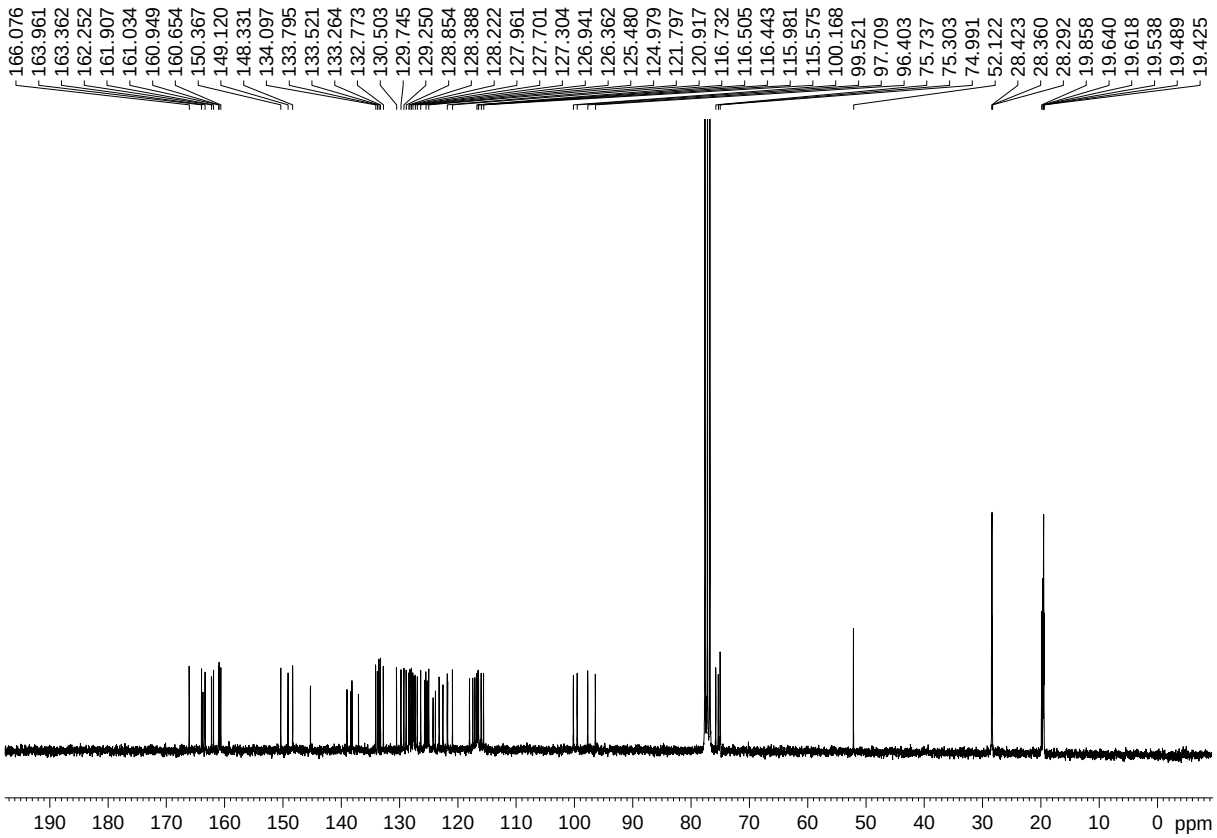

Figure S8. ^{13}C NMR spectrum (75 MHz, $CDCl_3$) of oligomer **5**.

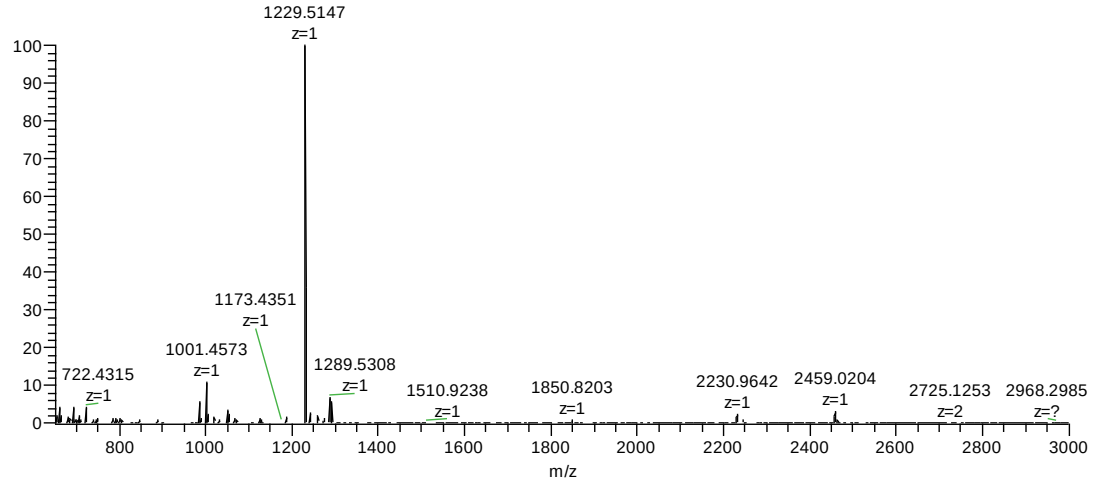

Figure S9. ESI+ HRMS spectrum of compound **5**.

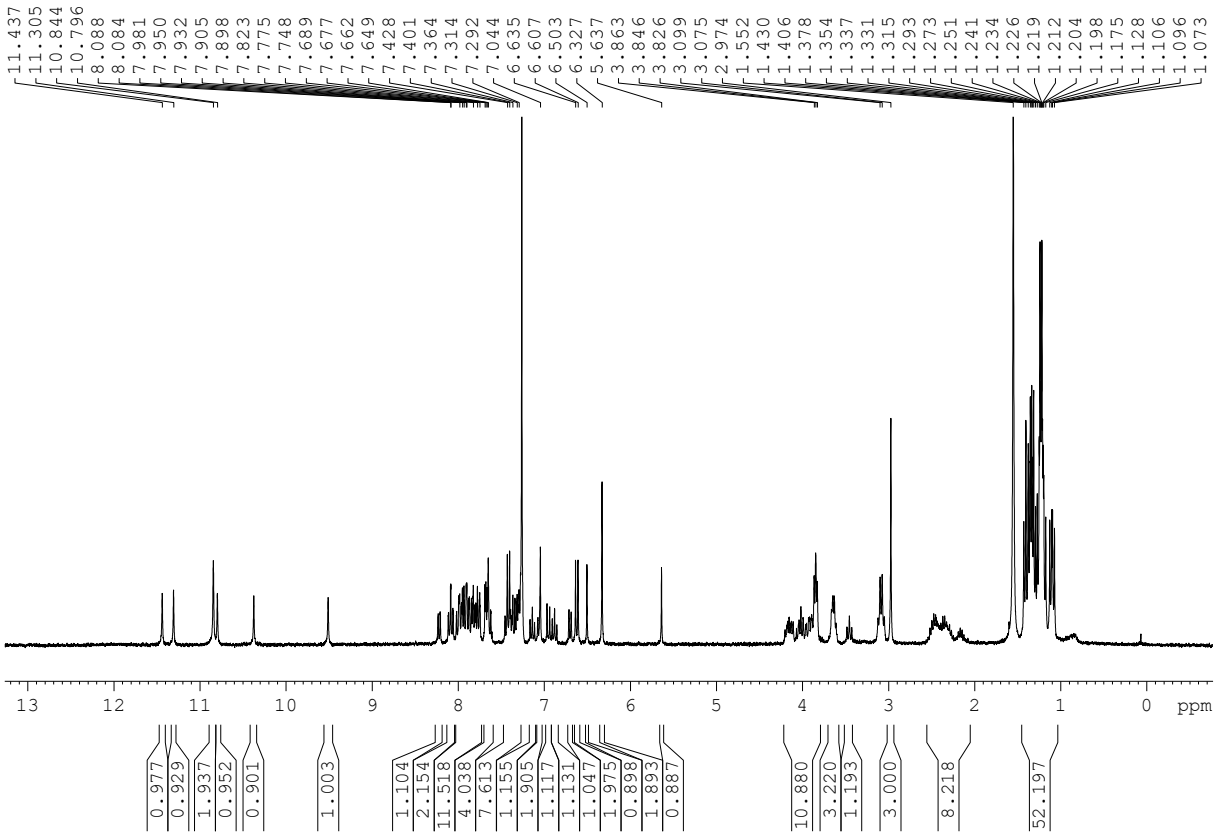

Figure S10. ^{1}H NMR spectrum (300 MHz, $CDCl_3$) of oligomer **6**.

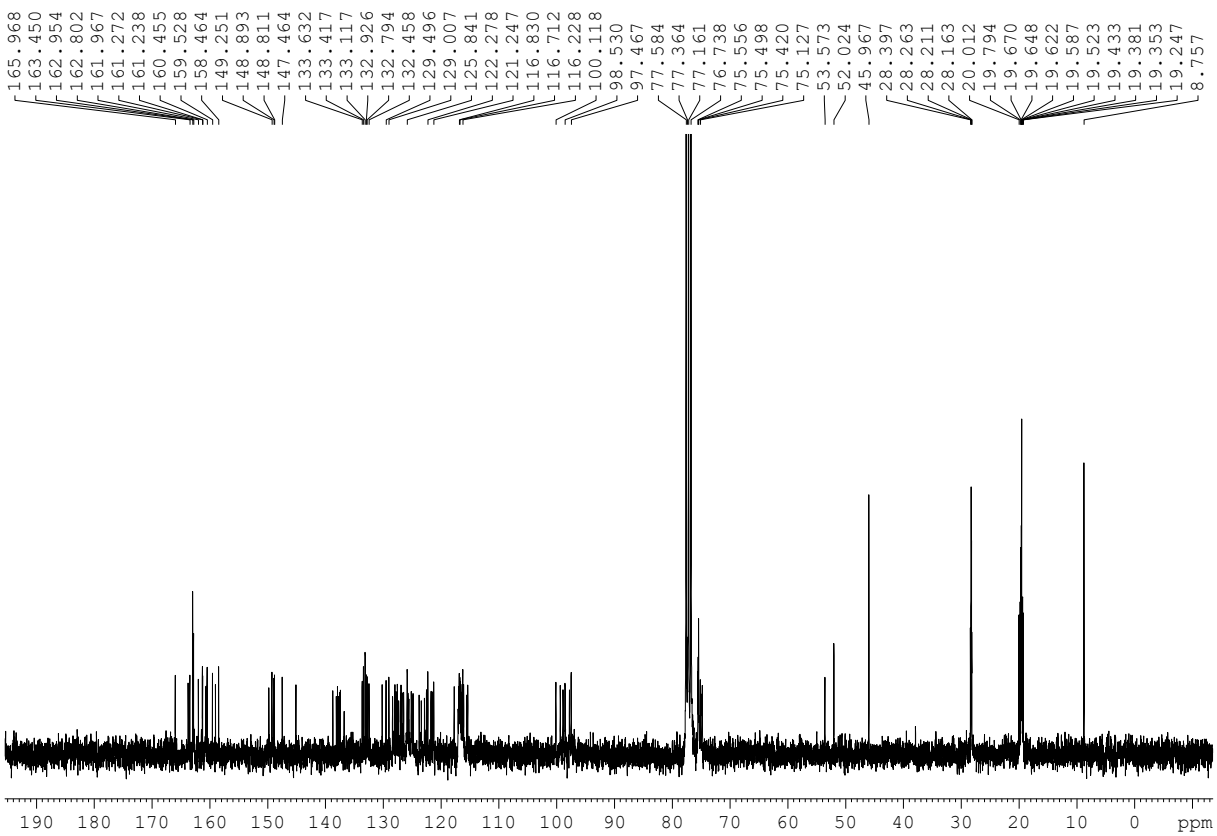

Figure S11. ^{13}C NMR spectrum (75 MHz, $CDCl_3$) of oligomer **6**.

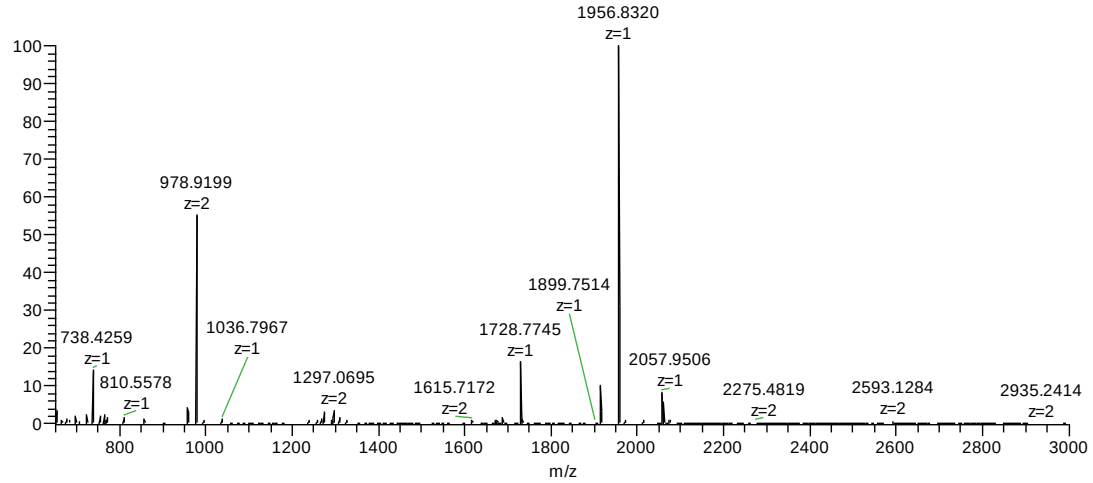

Figure S12. ESI+ HRMS spectrum of compound **6**.

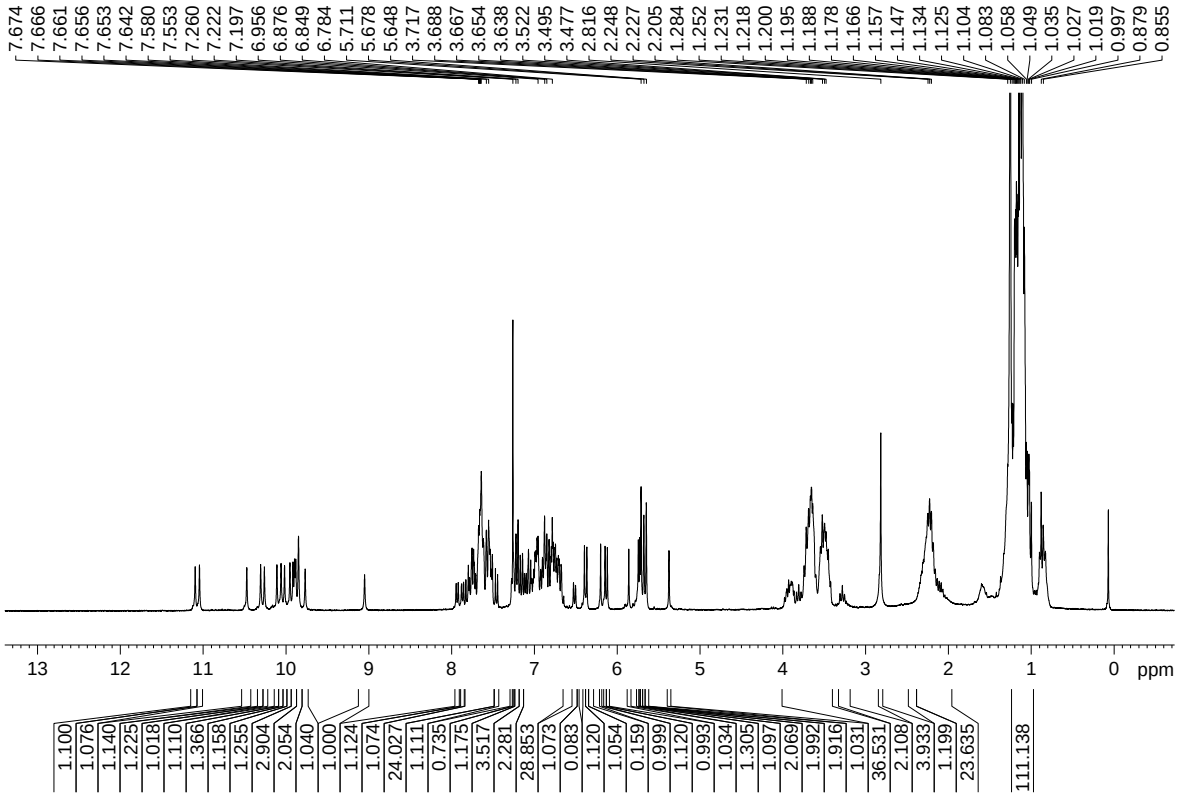

Figure S13. ^{1}H NMR spectrum (300 MHz, $CDCl_3$) of oligomer **7**.

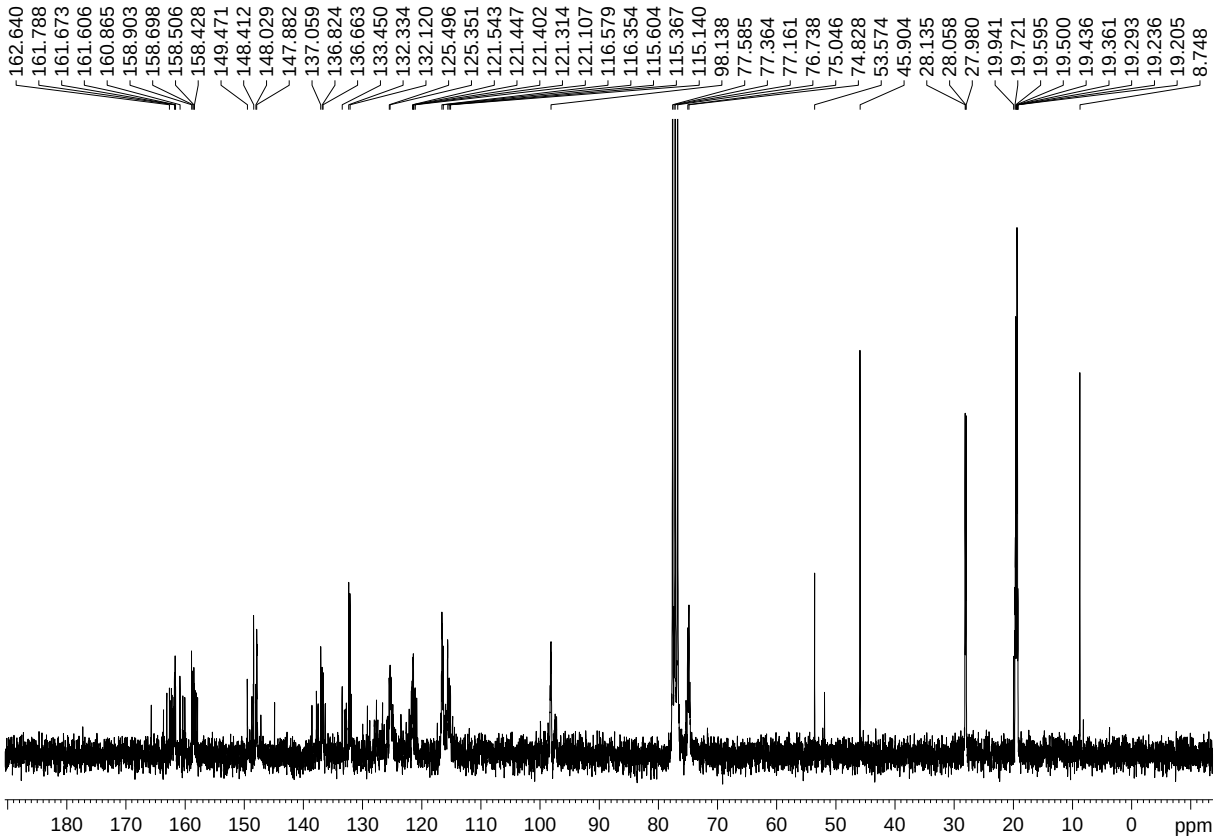

Figure S141. ^{13}C NMR spectrum (75 MHz, $CDCl_3$) of oligomer **7**.

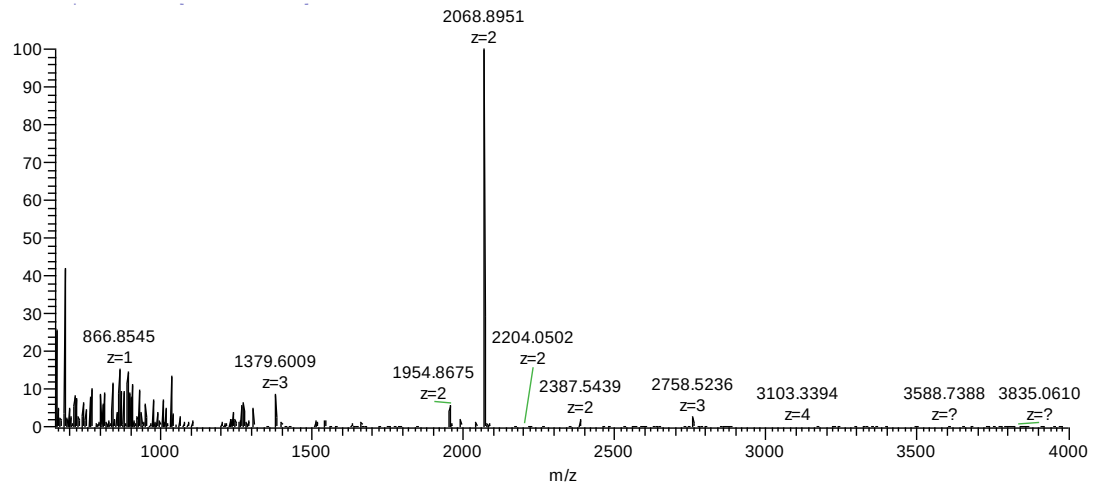

Figure S15. ESI+ HRMS spectrum of compound **7**.

8. References

1 a) T. Qi, T. Deschrijver and I. Huc, *Nat. Protoc.*, 2013, **8**, 693-708; b) X. Li, N. Markandeya, G. Jonusauskas, N. D. McClenaghan, V. Maurizot, S. A. Denisov and I. Huc, *J. Am. Chem. Soc.*, 2016, **138**, 13568-13578.

2 a) N. Delsuc, T. Kawanami, J. Lefeuvre, A. Shundo, H. Ihara, M. Takafuji and I. Huc, *ChemPhysChem*, 2008, **9**, 1882-1890; b) J. Wang, B. Wicher, A. Méndez-Ardoy, X. Li, G. Pecastaings, T. Buffeteau, D. M. Bassani, V. Maurizot and I. Huc, *Angew. Chem. Int. Ed.*, 2021, **60**, 18461-18466.

3 O. V. Dolomanov, L. J. Bourhis, R. J. Gildea, J. A. K. Howard and H. Puschmann, *J. Appl. Crystallogr.*, 2009, **42**, 339-341.

4 G. Sheldrick, *Acta Crystallogr., Sect. A*, 2015, **71**, 3-8.

5 G. Sheldrick, *Acta Crystallogr., Sect. C*, 2015, **71**, 3-8.

6 L. Rayleigh, *London, Edinburgh, Dublin Philos. Mag. J. Sci.,* 1882, **14** 184–186

7 R. B. Maximino, *Phys. Chem. Liq.*, 47, **5**, 475–486

8 V. Gabelica, S. Livet and F. Rosu, *J. Am. Soc. Mass Spectrom.*, 2018, **29**, 2189-2198

9 V. Calabrese, H. Lavanant, F. Rosu, V. Gabelica and C. Afonso, *J. Am. Soc. Mass Spectrom.*, 2020, **31**, 969-981

10 J. J. P. Stewart, *J. Mol. Model.*, 2013, **19**, 1-32.

11 Frisch, M. J.; Trucks, G. W.; Schlegel, H. B.; Scuseria, G. E.; Robb, M. A.; Cheeseman, J. R.; Scalmani, G.; Barone, V.; Petersson, G. A.; Nakatsuji, H.; Li, X.; Caricato, M.; Marenich, A. V.; Bloino, J.; Janesko, B. G.; Gomperts, R.; Mennucci, B.; Hratchian, H. P.; Ortiz, J. V.; Izmaylov, A. F.; Sonnenberg, J. L.; Williams; Ding, F.; Lipparini, F.; Egidi, F.; Goings, J.; Peng, B.; Petrone, A.; Henderson, T.; Ranasinghe, D.; Zakrzewski, V. G.; Gao, J.; Rega, N.; Zheng, G.; Liang, W.; Hada, M.; Ehara, M.; Toyota, K.; Fukuda, R.; Hasegawa, J.; Ishida, M.; Nakajima, T.; Honda, Y.; Kitao, O.; Nakai, H.; Vreven, T.; Throssell, K.; Montgomery Jr., J. A.; Peralta, J. E.; Ogliaro, F.; Bearpark, M. J.; Heyd, J. J.; Brothers, E. N.; Kudin, K. N.; Staroverov, V. N.; Keith, T. A.; Kobayashi, R.; Normand, J.; Raghavachari, K.; Rendell, A. P.; Burant, J. C.; Iyengar, S. S.; Tomasi, J.; Cossi, M.; Millam, J. M.; Klene, M.; Adamo, C.; Cammi, R.; Ochterski, J. W.; Martin, R. L.; Morokuma, K.; Farkas, O.; Foresman, J. B.; Fox, D. J., Gaussian 16 Rev. B.01. Wallingford, CT, 2016.

12 M. F. Mesleh, J. M. Hunter, A. A. Shvartsburg, G. C. Schatz and M. F. Jarrold, *J. Phys. Chem.*, 1996, **100**, 16082.